Research

Burn risk modeling and cost estimation for surface grinding optimization

Taiwo D Fasae*[1], Richard J Povinelli[1]

* Corresponding author taiwofasae@gmail.com
1 Department of Electrical and Computer Engineering, Marquette University, Milwaukee, USA.

Abstract

Achieving zero defects in surface grinding depends heavily on selecting process parameters that minimize the risk of thermal damage, as these parameters directly affect heat generation and its effects. Traditional defect minimization methods typically rely on constraint-based optimization, where certain parameter ranges considered prone to burn are excluded using thermal models. This binary treatment of thermal damage – assuming a part either burns or does not – often eliminates cost-effective parameter combinations, thus overlooking more nuanced trade-offs. This paper presents a novel cost model that incorporates burn probability and thermal risk estimation by offering a quantitative framework for optimizing grinding parameters towards overall cost efficiency, whilst considering defects. Unlike traditional threshold-based approaches, this model accounts for varying levels of thermal risk rather than applying rigid burn/no-burn constraints. Experiments were conducted using a horizontal spindle reciprocating table surface grinder equipped with a 350 mm diameter cubic boron nitride (cBN) wheel. Grinding tests were performed on Inconel 718 steel workpieces (85 mm x 203 mm x 11 mm) with a 2 mm depth of cut. From these trials, models for surface roughness, grinding force, power consumption, and burn probability were developed. Our results show that conventional defect-avoidance strategies often discard viable parameter settings by relying heavily on arbitrary thermal thresholds and failing to consider cost implications. In contrast, the proposed burn cost model enables a more flexible, robust, risk-aware, and value-driven optimization process by incorporating the cost of the workpiece into decision-making. This shift from qualitative to quantitative treatment of thermal risk enables smarter trade-offs between defect risk and operational efficiency.

Keywords
surface grinding, thermal damage, grinding burn, burn detection, optimization, probability

1 Introduction

Surface grinding is the preferred method for achieving precision in cutting, flattening, and finishing operations due to its accuracy, cost-effectiveness, and versatility. For example, the stringent dimensional and surface quality requirements of silicon wafers used in high-performance electronics are best met through surface grinding. In aerospace manufacturing, where the precision of engine components is critical and errors can be costly, surface grinding ensures the necessary accuracy and finish. Given its role in producing high-quality surfaces with tight tolerances, careful selection of grinding parameters is essential to maintain both performance and cost efficiency.

In surface grinding, cost efficiency is often pursued by minimizing thermal defects, which helps reduce machining losses. In semiconductor manufacturing, silicon wafers must not only meet strict dimensional tolerances but also maintain their structural integrity. Likewise, aerospace components must retain their metallurgical properties—any thermal alteration can render them unusable. This is

especially critical for high-value parts like turbine disks, which can cost up to $1 million each. The risk of excessive heat generation from grinding friction and the potential financial consequences highlights the need for thorough thermal damage analysis when selecting optimal grinding parameters.

Although thermal damage costs can account for a significant portion of total machining costs, it is often overlooked in cost analysis [1–6]. When thermal damage is treated as a process constraint, optimization typically occurs in two stages: first to avoid defects, and then to minimize cost, or both simultaneously. This approach is common for several reasons. First, thermal interactions are difficult to model accurately, thereby making it challenging to estimate thermal damage losses during cost analysis. Second, the cost of thermal damage is so high relative to total cost that practitioners often avoid any process settings that carry even a slight risk of damage. However, this constraint-based approach can eliminate parameter choices that, while more expensive to grind, are ultimately more cost-effective due to their lower risk of thermal damage. In this work, we advocate for a selection strategy that considers total effective cost and incorporates risk-aware decision-making—specifically, one that explicitly accounts for thermal damage losses in the optimization objective.

In this paper, we examined two approaches to parameter selection: the conventional threshold-based elimination method and a proposed thermal risk-adjusted burn cost model. We compare their respective strengths and limitations, particularly in how they both influence grinding parameter choices.

The remainder of the paper is structured as follows: Section 2 reviews existing surface grinding optimization techniques and traditional methods for mitigating thermal damage during parameter selection. Section 3 introduces the thermal damage cost model and the concept of burn probability. Section 4 outlines the grinding process model, including cost formulations, constraint definitions, and simplifications to the optimization objective. Section 5 presents a case study involving a 350 mm diameter cubic boron nitride (cBN) wheel and an 85 mm by 203 mm by 11 mm steel workpiece. Section 6 discusses the results of cost adjustment under thermal risk, and Section 7 concludes the paper.

1.1 State of the art in thermal damage avoidance

Grinding parameter selection involves choosing appropriate wheel speeds, work speeds, feed rates, and cut depths for every facet of the grinding operation. These parameters directly affect key outcomes such as total cost, thermal damage (burn), and surface finish. In the pursuit of cost efficiency, parameter selection strategies have progressed from traditional rule-based methods [7] to advanced optimization techniques designed to address the inherent complexities of the grinding process. This pursuit has also driven research into grinding heat interactions, with efforts focused on capturing thermal effects and detecting thermal damage. Thermal modeling has evolved significantly – from early approaches based on residual stress [8–10], temperature [4, 11, 12], optics [13, 14], acoustics [15, 16], to more recent applications of physics-based models [11, 17], signal processing, and machine learning. Overall, the goal remains to identify parameter combinations that minimize total cost while satisfying constraints on quality and process reliability.

One of the earliest efforts to formulate grinding costs was by Field et al. [1], who proposed a detailed cost function later applied by Wen et al. [2] to optimize production costs and material removal rates. Building on this, Amitay et al. [18] and Lee et al. [19] developed control strategies for optimizing sequences of grinding operations, including larger batch processing cycles [20]. Recent advancements in artificial intelligence, computational power, and data acquisition have further improved grinding process modeling, with machine learning techniques such as neural networks and backpropagation showing promising results [21, 22]. Lee et al. [5, 23] also demonstrated the effectiveness of evolutionary computation in parameter selection, emphasizing the reduced computation time and improved solution quality offered by evolutionary strategies. However, despite these advances in surface grinding

optimization, the cost implications of thermal damage remain largely absent from most total cost analyses.

Thermal damage is a critical concern in grinding and has prompted the development of various strategies aimed at improving cost efficiency by minimizing heat-induced defects. A widely adopted approach is the two-stage grinding method, which combines an aggressive rough grinding phase for high material removal with a subsequent finish grinding phase focused on surface quality [2]. Additional strategies directly influenced by thermal considerations include shallow grinding, creep feed grinding [12], dry and wet grinding modes [24], and High Efficiency Deep Grinding (HEDG) [12, 25–27]. Notably, Rowe's work in 2001 [25] and 2013 [28] emphasized a precautionary approach by identifying parameter ranges associated with a high risk of thermal damage and excluding them from consideration. Ultimately, grinding parameter selection is shaped by cost-performance trade-offs and is evaluated based on its effectiveness in minimizing total process costs—including losses due to thermal damage.

Thermal models, crucial in understanding heat interactions, are essential for minimizing thermal losses during grinding parameter selection. Models focused on heat transfer, temperature distribution [4, 11, 25], residual stress [8–10], and grinding energy [27] have proven effective in predicting thermal damage. Kruszynski et al. [8] explored the relationship between residual stress and thermal damage, while Hamdi et al. [9] and Lazoglu et al. [10] developed residual stress-based models as indicators of thermal distress. A notable advancement came from Malkin et al., who introduced the moving heat source model [11, 29], identifying a maximum temperature zone as a critical threshold for thermal damage classification. Building on this, subsequent studies introduced concepts such as energy partitioning (as a function of burn) [11], temperature- and energy-based burn thresholds [26], and grinding burn process limits [30]. While these models have significantly advanced our understanding of grinding thermal dynamics, effective parameter selection still demands more nuanced thermal damage information, particularly insights drawn from signals and time-series data.

Recent advances in machine learning, computational power, and signal instrumentation have significantly improved the precision of thermal dynamics capture and modeling in grinding processes [31]. Contemporary thermal models now incorporate a variety of real-time signals—including power [30], energy [27], force, optical reflections [13, 14], acoustic emissions [15, 16], and induced magnetism [13, 32] —collected during grinding operations. Magnetic signals, such as those derived from Barkhausen noise and eddy currents, have been particularly effective in detecting thermal damage by identifying changes in the material's magnetic field [13, 32, 33]. Additionally, Guo et al. [34] and Sauter et al. [15] developed burn detection models based on time-varying force and power measurements captured via dynamometers and wattmeters, respectively. Similarly, optical signal-based models have been developed by Kovacs and Khazi using reflections from the workpiece surface [13, 14]. While these models offer deeper insight into the onset and progression of thermal damage, their integration into a cost optimization framework aimed at simultaneously reducing grinding costs and thermal damage losses remains largely unexplored.

Despite their significant impact on overall cost, thermal damage losses have largely been excluded from total grinding cost analyses and parameter selection objectives. The prevailing strategy for addressing grinding burn is the threshold constraint approach, as summarized in **Table 1**, which outlines studies from the past decade. In several of these studies, burn avoidance is either neglected or addressed in a limited manner. For instance, one study [35] applies a penalty term for threshold violations, but the approach is overly generalized across different threshold types and fails to incorporate explicit thermal damage cost modeling. Unlike the constraint-based approach—which can overly restrict the parameter selection space—a cost-based method enables more nuanced trade-offs between grinding efficiency and thermal damage risk. Furthermore, existing thermal models typically classify burn as a binary outcome (present or absent) [15, 26, 30, 32, 34] or into severity categories such as no burn, mild, and severe [6, 36]. These models can be redesigned to output burn probabilities,

enabling the estimation of expected thermal damage costs. In summary, a burn cost model provides a quantitative framework that balances economic efficiency with the risk of thermal damage, offering a more informed basis for parameter selection.

Table 1 Recent grinding optimization designs and respective burn avoidance strategies

Name	Workpiece material	Optimization objective	Grinding burn model	Burn avoidance strategy
Khosravi et al. 2023 [35]	NA	Sum of controller performance metrics	Probabilistic surrogate model of burn	Penalty for constraint violations
Kota et al. 2022 [37]	35NCD16	Avoid grind-induced burn	Nital etching and depth of white layer formation	Hardness constraint
Jamshidi et al. 2022 [38]	Inconel 718	Maximize material removal rate, MRR	Fused model of temperature and burn thickness	Surface burn limit constraint
Sauter et al. 2022 [39]	C45E, 20MnCrS5, 100Cr6	Maximize burn detection accuracy	Models of critical temperature and maximum temperature rise	Surface burn threshold constraint
Heinzel et al. 2021 [30]	AlSl1.7147, .7131, .6587	Minimize thermal defects	Grinding burn depth; maximum temperature rise	Burn constraint
Afsari et al. 2020 [40]	NA	Minimize production cost; maximize production rate	Critical temperature line model	Thermal damage constraint
Debnath et al. 2020 [41]	NA	Minimize machining time	Power limitation model	Power limitation constraint
Nametala et al. 2020 [21]	Inconel 751, DIN 1.4882, Sil1	Grinding wheel wear; material removal, cost per piece	NA	Enough cutting fluid
Maier et al. 2020 [4]	Tribo S25	Minimize production cost	Gaussian process regression of temperature	Max temperature constraint
Pereverzev et al. 2019 [42]	NA	Minimize cycle time	NA	Non-burn restriction
Patel et al. 2018 [43]	EN8 steel	Maximize grinding performance	NA	Ignored
Steffan et al. 2017 [44]	100Cr6 steel	Minimize thermal defects	Barkhausen noise analysis	Noise signal constraint
Jiang et al. 2016 [45]	AlSI 52.100 steel	Minimize errors in modeling force and temperature	FEM on heat flux distribution	Temperature field constraint

1.2 Thermal damage losses and risk probability

A comprehensive grinding cost analysis should account for the cost of discarding defective workpieces—including both the cost of the failed grinding process and the cost of thermal damage, which can exceed the grinding cost itself [28]. A workpiece is considered thermally defective when structural alterations occur due to excessive heat generated by friction between the grinding wheel and the workpiece. The term surface burn refers broadly to all undesirable surface changes caused by grinding-induced heat, typically characterized by oxidizing burn [24, 46]. These changes may include surface softening or re-hardening, the development of tensile residual stresses, thermal expansion, and chemical reactions—each of which can compromise final workpiece integrity.

Strategies for minimizing thermal damage generally fall into two categories: qualitative and quantitative. The qualitative approach treats thermal damage as a risk to be avoided and employs threshold-based rules to eliminate parameter combinations associated with burn. The selection criteria aim to maintain a safe margin from the burn threshold, thereby minimizing the likelihood of thermal damage. While this method can be effective, it relies on accurate knowledge of the burn threshold and the appropriate safety margin—factors that can be more systematically addressed through quantitative approaches.

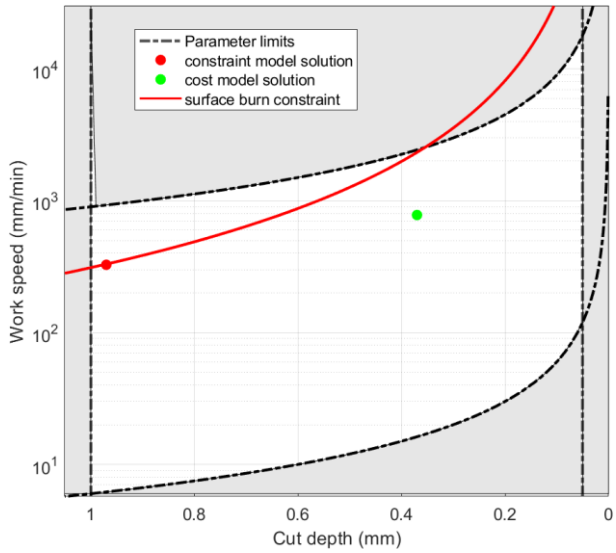

Fig. 1 Qualitative approach to thermal damage avoidance. The parameter combination is selected to be on the "safe" side of the burn threshold line (red).

On the other hand, the quantitative approach estimates the impact of thermal damage by assigning a probability to the occurrence of burn and translating it into an expected cost. This approach proves especially valuable in comprehensive grinding cost analysis, as it enables a more informed and risk-aware parameter selection process. To incorporate thermal damage into the total cost framework, we define a weighted cost function that balances grinding cost and burn cost ($w \in [0,1]$ represents the relative importance assigned to grinding cost versus burn cost):

$$Total\ Cost = w \cdot Cost_{grinding} + (1 - w) \cdot Cost_{burn}. \quad (1)$$

The cost of burn is determined by the product of the probability of a burn event and the value of the workpiece. A burn event occurs when excessive thermal exposure renders a workpiece unusable. If

m identical grinding tasks were performed and $B_k \in \{0,1\}$ denotes the burn event for task k (0 = no burn, 1 = burn), the empirical probability of burn is

$$\mathbb{P}\{burn\} = \frac{1}{m}\sum_{k=1}^{m} B_k \,. \tag{2}$$

The burn cost formulation must satisfy two key criteria:

1. It must be continuously valued and differentiable.
2. It must incorporate all relevant grinding parameters.

Burn probability captures the thermal dynamics of the grinding process and serves as a practical risk, analogous to real-world metrics like burn rate [47].

The expected cost of burn is expressed as:

$$E[Cost_{burn}] = \mathbb{P}\{burn\} \cdot Cost_{burn} + \mathbb{P}\{no_{burn}\} \cdot Cost_{no_{burn}}, \tag{3}$$

Given that:

$$Cost_{no\_burn} = 0, \text{and} \tag{4}$$

$$Cost_{burn} = \text{workpiece value}, V. \tag{5}$$

Expression (3) simplifies to:

$$Cost_{burn} = \mathbb{P}\{burn\} \cdot V. \tag{6}$$

This formulation provides a burn cost estimate, which we later integrate into the total cost function to guide parameter selection toward minimizing overall cost. In the following section, we introduce our surface grinding system model.

2 Surface grinding system model

The grinding process is modeled as a sequence of passes, where each pass represents a complete traversal of the grinding wheel from one end of the workpiece to the other. This sequence is characterized by a set of parameters – wheel speed, depth of cut, and work speed – executed over N passes, as illustrated in **Fig. 2**.

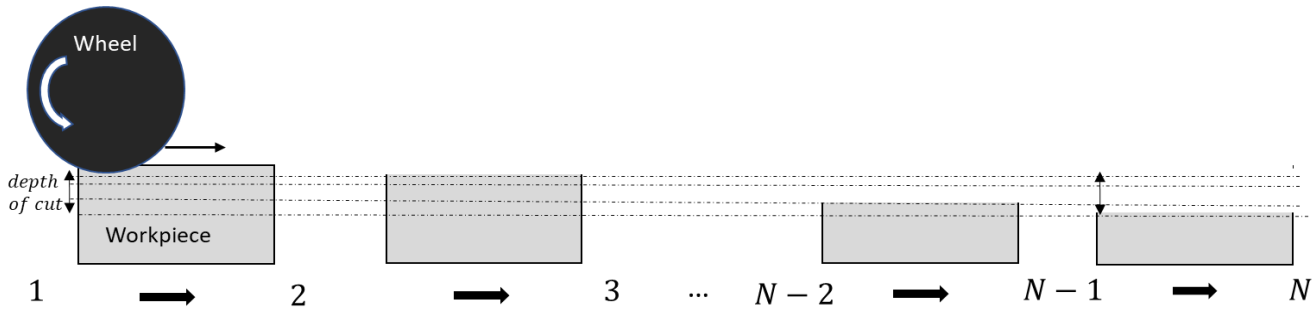

Fig. 2 A horizontal spindle reciprocating surface grinding configuration. The task is on the third pass with a_3 cut depth, $v_{w,3}$ work speed, and $v_{s,3}$ wheel speed.

This model is applicable to a wide range of grinding configurations, including cylindrical grinding, where the grinding length corresponds to the circumference of a full rotation of the workpiece about its axis. The grinding system can be summarized by three key components:

- **Inputs** – grinding parameters such as wheel speed, workpiece speed, and depth of cut,
- **Outputs** – performance metrics including grinding cost and surface burn outcomes, and
- **Process models** – mathematical representations that capture the underlying system dynamics.

System input

Let the set of parameters $(v_{w,i}, a_i, v_{s,i})$ represent the system input for grinding pass i. Then the process input set $\boldsymbol{x}$ is the union of all parameters across all passes N:

$$\boldsymbol{x} = \bigcup_{\boldsymbol{i=1}}^{\boldsymbol{N}} (v_{w,i}, a_i, v_{s,i}) . \tag{7}$$

Process cost

The total grinding cost across N passes with costs C_i for pass i is

$$C_{total} = C_1 + \cdots + C_{N-1} + C_N = \sum_{i=1}^{N} C_i . \tag{8}$$

The grinding cost C_i as a function of input set $(v_{w,i}, a_i, v_{s,i})$ and cost parameters in **Table 2** is given by Field et al. [1] as

$$C_i = Cost(v_{w,i}, a_i, v_{s,i}) = \frac{M}{60} \times R_t + \frac{M}{60}\left[\left(\frac{L_w}{1000 v_{w,i}}\right)\right] + C_s \times \frac{a b_w L_w}{G(\cdot)} . \tag{9}$$

The cost in equation (9) includes the time value of grinding and the amount of wheel material lost from the grinding and dressing action. While the costs of coolant delivery and dressing can be significant, they are constant across passes and insignificant, and as such, are excluded from our optimization analysis. The total cost from Equation (8) over N passes with parameter set $\boldsymbol{x}$ becomes the sum,

$$C_{total}(\boldsymbol{x}) = \sum_{i=1}^{N} Cost(v_{w,i}, a_i, v_{s,i}) . \tag{10}$$

Table 2 Process parameters

	Parameter	Description
Process Inputs	v_s, wheel speed	Rotational speed of the wheel, in meters per second (m/s)
	a, cut depth	Depth of material to be removed from the workpiece (mm)
	v_w, work speed	Translational speed of the workpiece in the grinding direction (mm/min)
	N, no. of passes	Complete wheel movements from workpiece end to end
	$v_{w,i}, a_i, v_{s,i}$	Work speed, depth of cut, and wheel speed for pass i
Process cost	M	Hourly cost of grinding, in \$/hr
	C_s	Unit cost of grinding wheel, in \$/mm^3
	L_w	Workpiece length, in mm
	b_w	Workpiece width, in mm
	R_t	Rapid traverse time, in seconds. These are 'empty' runs used to move the wheel back to the start position.
	$G(\cdot)$	Grinding ratio model

Process constraints

Process specifications such as surface finish and workpiece material preservation are captured using constraints. The traditional burn constraint ensures the grinding power P does not exceed the maximum power P_b, i.e., $P \leq P_b$. Similarly, the surface roughness constraint limits the average roughness value, R_a.

Table 3 System constraints for the grinding process

Monitoring variable	Constraint	
P	Below maximum power level P_b	$P \leq P_b$
R_{finish}	Not greater than surface finish R_a	$R_{finish} \leq R_a$

3 Process models

Process dynamics of force, power, grinding ratio, surface roughness, and burn detection, are examined highlighting their respective importance in **Table 4**. The models are developed using machine learning as outlined in the case study section.

Table 4 Process models and importance

Process variables	Importance
Tangential force and power	For estimating grinding power levels and grindability
Grinding ratio	For estimating the volume of wheel wear loss during grinding
Surface roughness	For assessing the surface finish
Burn detection	For avoiding and minimizing thermal damage

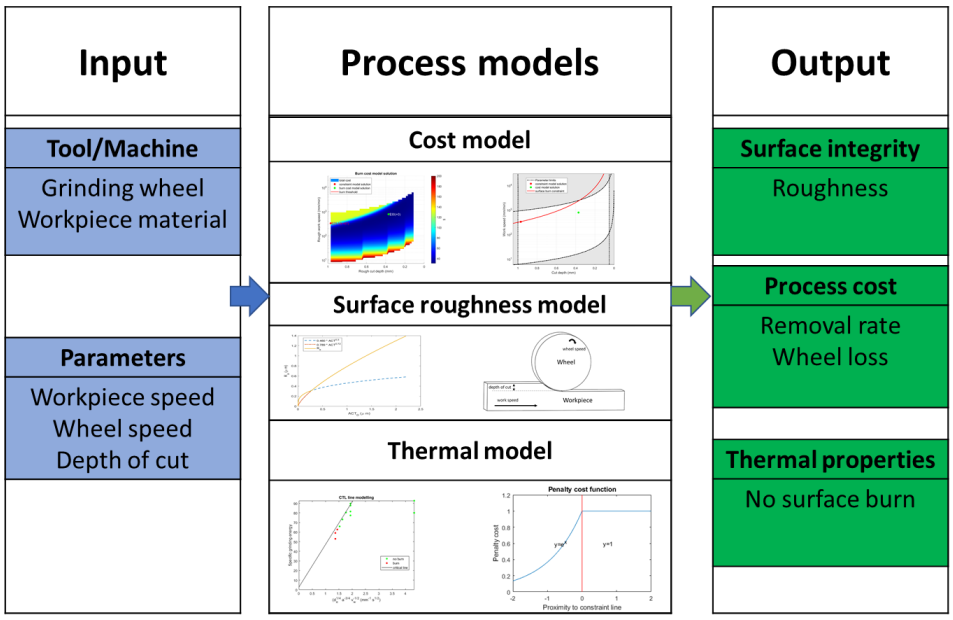

Fig. 3 System model for the surface grinding process

3.1 Frictional force and Power

Force and power models are helpful for estimating power levels and force profile during and at the end of a grinding pass. In addition, monitoring power levels is crucial to many thermal damage avoidance procedures. Let coefficients c_1, c_2, c_3, and c_4 apply to cut depth a, work speed v_w, wheel speed v_s, and wheel diameter d_s respectively. The generalized model [6] for tangential force is

$$F_t = F_0 a^{c_1} v_w^{c_2} v_s^{c_3} d_s^{c_4}. \tag{11}$$

Although monitoring variables like force and power is valuable for optimization, measuring grinding force is often more costly and complex than measuring grinding power, which can offer comparable insights. The grinding power P and tangential force F_t is related by the cutting velocity (wheel speed v_s) as [48]

$$P = F_t v_s. \tag{12}$$

3.2 Grinding ratio

As part of estimating the wheel material loss, the grinding ratio expresses the amount of workpiece material removed Vol_w for every unit of wheel material lost Vol_s and is given [28] as

$$G = \frac{Vol_w}{Vol_s}. \tag{13}$$

The grinding ratio sometimes is included as a maximization objective and, in other cases, only a specific value of grinding ratio is desired. The generalized grinding ratio model by Choi et al. [6] is

$$G = G_0 \left(\frac{v_w a}{v_s}\right)^{-g}. \tag{14}$$

3.3 Surface roughness

The surface roughness model captures process dynamics relating to the workpiece's surface finish [49], which is integral to process success and specifications, i.e., meets a specified value, R_a. Surface roughness according to Lindsay et al. [50] is

$$R_a = \begin{cases} 0.460 * ACT_D^{0.30} & 0.0254 \le ACT_D \le 0.254\ \mu m \\ 0.789 * ACT_D^{0.72} & 0.254 \le ACT_D \le 2.54\ \mu m \end{cases}, \tag{15}$$

with wheel diameter d_s, specific removal rate Q', work speed v_w, effective diameter D_e. The average chip thickness ACT_D is [50]

$$ACT_D = 4.9697 \left(\frac{d_s^{\frac{4}{7}} \cdot Q'^{\frac{5}{7}}}{v_w^{\frac{1}{7}} \cdot D_e^{\frac{2}{7}} \cdot v_s^{\frac{4}{7}} \cdot f^{0.83}} \right). \tag{16}$$

3.4 Burn detection and probability

Thermal damage is influenced by several key factors, including work speed v_w, wheel speed v_s, specific material removal rate Q', coolant delivery effectiveness [51], and wheel condition. For instance, increasing wheel speed elevates grinding energy input, which can increase the risk of thermal damage if the material removal rate is not properly managed. Conversely, reducing the work speed prolongs the

wheel's contact time with the workpiece, intensifying exposure to frictional heat and raising the likelihood of burn. To accurately capture heat dissipation and the mechanisms underlying thermal damage, our thermal model must account for these critical interactions.

According to Malkin et al. [11], a maximum temperature zone defines a threshold for thermal damage occurrence. As a function of process parameters, the critical specific energy u_c is [11, 48]

$$u_c = u_0 + BD_e^{1/4} a^{-3/4} v_w^{-1/2}, \tag{17}$$

and maximum grinding power $P_b = u_c Q$ as

$$P_b = u_0 b_w v_w a + BD_e^{1/4} a^{1/4} v_w^{1/2} b_w. \tag{18}$$

The intercept u_0 and slope B of the burn threshold line shown in Fig. 4 are derived using a classification algorithm, such as Support Vector Machines (SVM) [52, 53], equipped with probabilistic output capabilities. Each combination of input parameters is mapped to a corresponding burn probability, representing the likelihood that the given setting will result in thermal damage. Model evaluation results are presented in section 5.4.4.

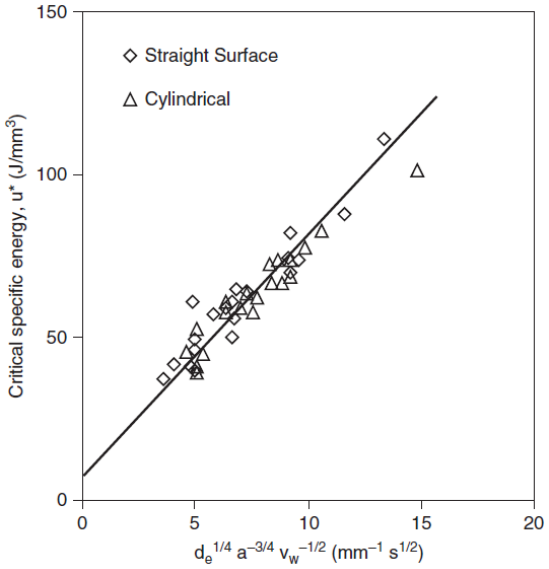

Fig. 4 Maximum temperature model showing the critical temperature line by Malkin et al. [11, 48]

3.5 Burn cost

Burn probability, defined as the likelihood of thermal damage, is directly influenced by grinding parameters that serve as inputs to the grinding system. We revisit the burn threshold formulation proposed by Malkin et al. [11], which establishes a maximum allowable grinding power P_b such that thermal damage is avoided when the actual grinding power P satisfies $P \leq P_b$ [11]. Both P_b and P are functions of work speed, cut depth, and wheel speed [11, 18, 20]. Since the threshold P_b governs the burn outcome, it implies the existence of a function f that maps these parameters to a corresponding burn probability, thereby quantifying the risk of thermal damage under varying operating conditions.

For our grinding system, the burn probability during grinding pass i, given input parameters $(v_{w,i}, a_i, v_{s,i})$ is modeled as:

$$\mathbb{P}_i\{burn\} = f(P_i \leq P_b) = f(v_{w,i}, a_i, v_{s,i}). \tag{19}$$

The overall burn probability across N passes (assuming mutually exclusive burn events) is

$$\mathbb{P}\{burn\} = 1 - \mathbb{P}\{no\ burn\} = 1 - \prod_{i=1}^{N}(1 - \mathbb{P}_i\{burn\})\,. \tag{20}$$

The expected cost of burning a workpiece of value V is

$$Cost_{burn} = \mathbb{P}\{burn\} * V. \tag{21}$$

4 Optimization objective

We define the optimization objective for two thermal damage avoidance scenarios: the qualitative approach using burn constraint threshold, and the quantitative approach using burn cost estimation and total cost inclusion. Let $R_{a,f}$ be the surface roughness for the final pass, R be the target surface roughness value, P_i denote the grinding power during pass i, P_b be the maximum power limit from thermal damage, and $Cost_{burn}$ denote the cost of burn. The revised objectives for both cases are shown in **Table 5**.

Table 5 Optimization objectives for qualitative (burn constraint) and quantitative (burn cost) approaches

Qualitative approach (Burn constraint threshold)	**Quantitative approach (Burn cost estimation)**
minimize: $\min_x\ Cost_{grinding}$	*minimize:* $\min_x \left[Cost_{grinding} + Cost_{burn}\right]$
subject to:	*subject to:*
i. surface roughness limit, $R_{a,f} \le R$, and ii. thermal damage absent, $P_i \le P_b$.	surface roughness limit, $R_{a,f} \le R$.

Rough and finish grinding. Following initial experimentation on the grinding system and optimization formulation, the two-stage grinding model (rough-aggressive followed by meticulous-finish) is adopted. Here,

i. the surface finish constraint applies only to the final pass, and
ii. all rough stage passes have identical parameters.

Let $v_{w,r}, a_r$ and $v_{s,r}$ denote the work speed, cut depth, and wheel speed for the rough passes, and $v_{w,f}, a_f$ and $v_{s,f}$ denote the work speed, cut depth, and wheel speed for the finish stage. Denoting n_r as the number of roughing passes (one less than the total number of passes), the grinding parameter set $\boldsymbol{x}$ becomes

$$\boldsymbol{x} = \left[v_{w,r}, a_r, v_{s,r}, n_r, v_{w,f}, a_f, v_{s,f}\right], \tag{22}$$

with number of passes $N = n_r + 1$. Subsequently, the grinding cost becomes

$$Cost(\boldsymbol{x}) = \sum_{i=1}^{N} Cost\left(v_{w,i}, a_i, v_{s,i}\right) = \left[Cost\left(v_{w,r}, a_r, v_{s,r}\right) * n_r\ + Cost\left(a_f, v_{w,f} v_{s,f}\right)\right], \tag{23}$$

and the probability of burn from equation (17),

$$\mathbb{P}\{burn\} = 1 - \left[(1 - \mathbb{P}_r\{burn\})^{n_r} \cdot \left(1 - \mathbb{P}_f\{burn\}\right)\right]. \quad (24)$$

The two-stage grinding simplification effectively reduces the degrees of freedom (DOF) of the system input from (three input variables each pass for possible N_{max} passes)

$$DOF = 3 * N_{max}$$

to

$$DOF = 7.$$

Optimization algorithms explored include gradient descent [2, 54, 55] and evolutionary algorithms [3, 5, 21]. Gradient descent iteratively adjusts parameters in the direction of the gradient until a locally optimal solution is reached, while evolutionary algorithms simulate biological evolution to identify candidate solutions that best satisfy the objective. In both cases, the search process concludes with an optimal combination of parameters that minimizes the objective. Given that our objective function is convex, gradient descent is well suited for this problem. For non-convex objectives with multiple local minima, probabilistic methods such as simulated annealing or Bayesian optimization would be more appropriate.

5 Case Study

5.1 Grinding configuration, Machine tool, and Workpiece specifications

The data used in this study is obtained from grinding operations conducted in a horizontal spindle reciprocating table setup depicted in Fig. 5. The machine consists of a cubic boron nitride (cBN) abrasive wheel measuring 350 mm in diameter. The workpiece material is an Inconel 718 steel measuring 203 mm long, 10.6 mm wide, and 85 mm tall. The wheel's width is at least double that of the workpiece, eliminating the need for cross feed action. Each grinding task involves making cut depths of 2 mm on a workpiece and each time with different values of work speeds, number of passes, and cut depths per pass. Machine configurations, workpiece parameters, and cost parameters are detailed in **Table 6**. The operating (machine) limits for process inputs are provided in **Table 7**.

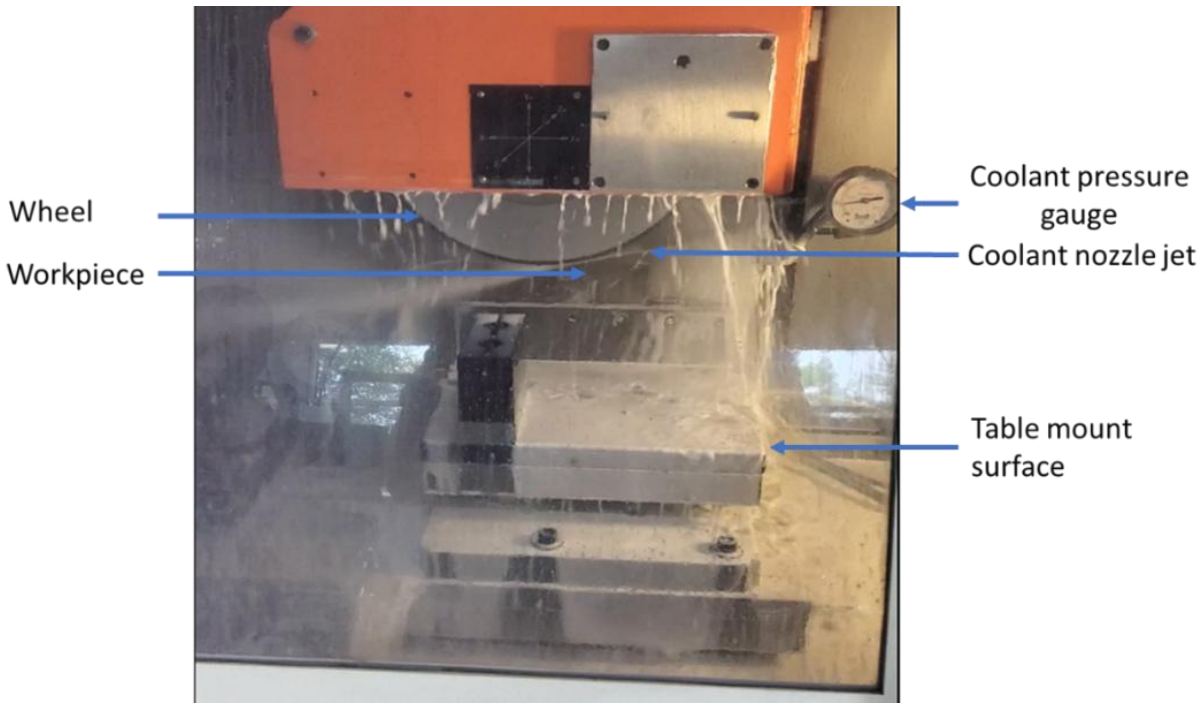

Fig. 5 The grinding machine, wheel, and workpiece setup in use

Table 6 Grinding configuration for the machine, workpiece, and cost

Machine	Wheel	Grinding wheel specification, S_s	Bates Vit cBN
		Wheel diameter, D_s (mm)	350
		Average abrasive diameter, d (mm)	0.126
		Abrasive grain fraction, f	0.38
		Wheel thermal conductivity, β (W/mK)	240
	Grinding	Grind direction	Down grind
		Chip energy, e_{ch} (J/mm^3)	6.0
		Abrasive grain radius, r_0 (μm)	15
		C-factor, C	0.75
Workpiece	Dimensions	L_w, Length of workpiece (mm)	203
		B_w, Width of workpiece (mm)	10.6
		Height of workpiece (mm)	85
	Specifications	a_{eT}, total cut depth (mm)	2.0
		R_a, target surface roughness (μm)	1.8
	Properties	Material	Inconel 718
		Hardness (HRC)	47
		Thermal conductivity, k_w (W/mK)	9.9
		Density, ρ_w (kg/M^3)	8190
		Specific heat capacity, $c_w(J/kg \cdot K)$	425
Cost		M, Hourly cost ($/hr)	200
		C_s, Wheel material cost ($/mm^3$	0.27
		Workpiece value ($)	200

Table 7 Operating ranges and process constraints

Parameters	Units	Requirements
Specific removal rate, $Q' = v_w a$	(mm^3/min)/mm	[0.1, 15.0]*
Cut depth, a	mm	[0.05, 1.00]
Work speed, v_w	mm/min	[6, 30000]
Wheel speed, v_s	m/s	[10, 70]

*[a, b] denotes a and b as lower and upper bounds for parameter

5.2 Grinding experiments

15 experiments were conducted with input parameters selected as follows. First, parameters were selected with varying likelihoods of surface burn as advised by a grinding domain expert. Second, the work speeds, wheel speed, and cut depths were selected as constant across passes, i.e., all grinding passes are identical. Only four parameters defined a grinding task: wheel speed v_s, cut depth a, work speed $v_w = \frac{Q'}{a}$, and number of passes N, such that total cut depth $a_{total} = N * a$. After each grinding task, the presence or absence of visible burn was recorded. In addition, power signals were acquired using a wattmeter setup comprising a National Instrument DAQ digitization module. Sensing systems such as the DAQ module provide 24-bit 32-channel digital outputs and bit rate of 250 bit/seconds [56]. The variables recorded are listed in **Table 8**. The power signals are further processed for modeling.

Table 8 Process parameters for the grinding tasks

Input parameters	Monitored process variables	Process output/outcomes
Work speed/pass, v_w	Power signal	Coolant burnout
Wheel speed, v_s	Average power	Surface burn
Cut depth/pass, a		Surface roughness
Number of passes, N		

5.3 Signal processing and transformation

Power signals acquired for the grinding tasks are amplitude adjusted to remove offset such as the no-load power levels. The signals are detrended to remove trends caused by vertical adjustment of the grinding wheel due to varying workpiece heights. The signals are also filtered for noise or high-frequency content using the standard moving average (SMA) operator. To calculate the average power for each grinding pass, the beginning and ending of the signals are first identified using derivatives (A positive derivative signals the start of the grinding pass, and a negative derivative signals the end.) Then the partitioned signals are averaged over the respective time periods. Time domain features such as mean, standard deviation, peak-to-peak amplitude, root mean square (RMS), and integral measurements were considered.

5.4 Machine learning and model evaluation

The process models are developed as follows.

5.4.1 Force and Power

Grinding force is derived using the generalized force model of equation (11). With k as constant and coefficients c_1, c_2, c_3, and c_4 for cut depth a, work speed v_w, wheel speed v_s, and wheel diameter d_s, respectively, the generalized model from equation (11) is

$$logF_t = log\ k + c_1 \log\ a + c_2 \log\ v_w + c_3 \log\ v_s + c_4 \log\ d_s\,. \tag{25}$$

The tangential force F_t is computed using equation (12): $F_t = \frac{P}{v_s}$ using recorded values of wheel speed v_s and average power P. The resulting force model with $k = e^{1.749}$ is

$$F_t = k\ a^{0.896} v_w^{0.667} d_s^{-0.151}, \tag{26}$$

with R^2 of 0.991. The regression coefficient for v_s is 0 as expected, since wheel speeds were kept constant across all tasks.

5.4.2 Grinding ratio

The grinding ratio is a key metric for quantifying wheel wear during a grinding operation. Using the model proposed by Choi et al. [6], along with a linear system of equations derived from the data in **Table 9** the grinding ratio model is expressed as

$$G = 14.0\ h_{eq}^{-0.13}. \tag{27}$$

Table 9: Experimental data for computing grinding ratio

#	Wheel diameter (mm)	Equivalent chip thickness $h_{eq}\ (mm)$	Radial wheel depth (um)	Volume of wheel removed $VOL_S\ (mm^3)$	Volume of work removed $VOL_W\ (mm^3)$	Grinding ratio, $G = \frac{VOL_W}{VOL_S}$
1	349.5	5×10^{-5}	5.0	55.8	2844	50.9
14	350.0	2.5×10^{-4}	4.0	46.6	1917	41.1

5.4.3 Surface roughness

In our case study, data for surface roughness were not collected. Instead, we borrowed the surface roughness model derived from the work of Lindsay et al. [57] as

$$\mathrm{R_a} = \begin{cases} 0.4587 T_{ave}^{0.30}\ for\ 0 < T_{ave} < 0.254 \\ 0.7866 T_{ave}^{0.72}\ for\ 0.254 < T_{ave} < 2.54 \end{cases} \tag{28}$$

with

$$T_{ave} = 11.095\ d_s^{\frac{4}{7}} a^{\frac{5}{7}} v_s^{\frac{1}{7}}. \tag{29}$$

5.4.4 Burn modeling and probability

In each experiment, the presence or absence of surface burn is determined using X-ray Diffraction (XRD) to verify the thermal condition of the workpiece post-grinding. Data from 15 experiments are used to develop the Critical Temperature Line (CTL) model [48]. A Support Vector Machines (SVM) algorithm is employed to identify the threshold line that separates “burn” from “no burn” data points, characterized by an intercept and slope. To ensure consistency with the underlying physics of grinding heat as defined in the CTL model [48], two constraints are applied: (1) the intercept

u_0 is physically constrained to 0.45 times the chip energy e_{ch}, and (2) the slope must lie within a physically plausible range, bounded by the maximum and minimum slopes formed by all data points, and must conform to grinding heat transfer behavior.

The optimization objective is the hinge loss function [58], as used in the SVM algorithm and illustrated in Fig. 6. The final calibrated values for the CTL model are: intercept $u_0 = 0.45, e_{ch} = 2.70\ J/mm^3$ and slope $B = 43.75\ Jmm^{-2}s^{-0.5}$. The resulting CTL model is plotted in Fig. 7.

Burn probabilities are derived from the probabilistic output of the SVM algorithm [52, 53], using a sigmoid function commonly employed in probabilistic interpretations of machine learning classifiers. In this context, $u - e_c$ represents the distance between the specific grinding energy u and its corresponding critical energy threshold e_c, the point at which thermal burn is expected to occur given the input parameter set.

$$P\{burn\} = \sigma(u - e_c) = \frac{1}{1 + e^{-(u-e_c)}}. \tag{30}$$

The derivation of models for grinding power, grinding ratio, surface roughness, and burn detection completes the grinding model which we further use for optimization. This is summarized in **Table 10.**

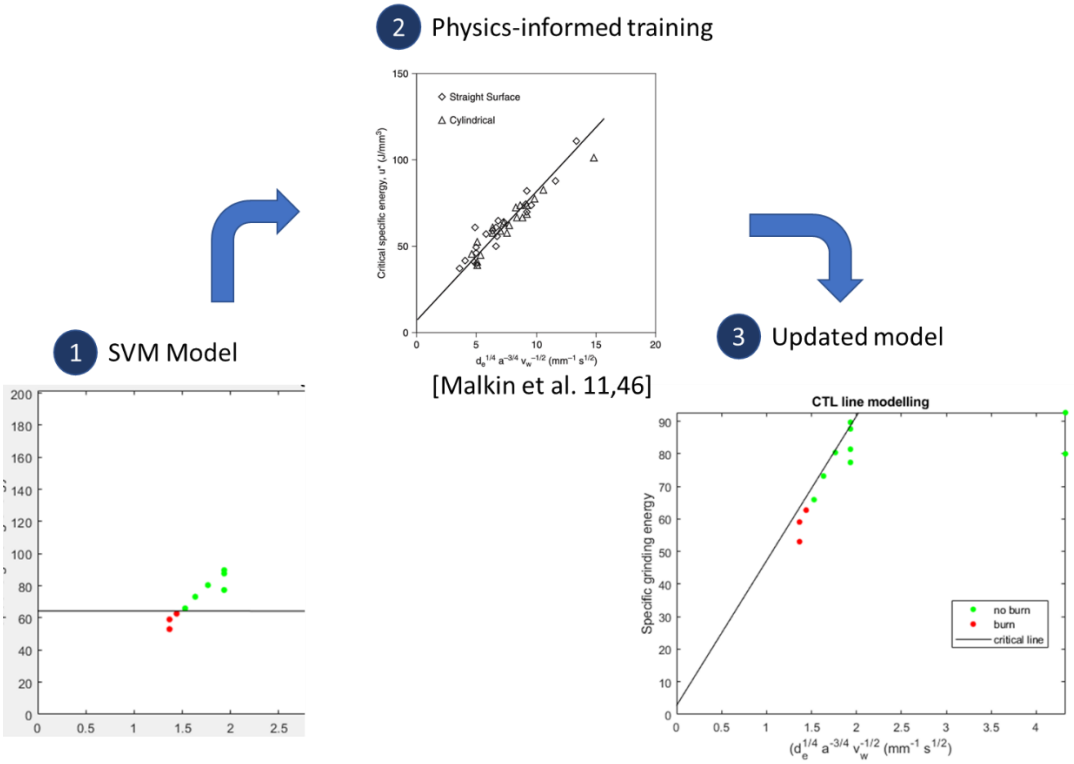

Fig. 6 Physics-informed training for burn detection development. Physical constraints of intercept (chip energy e_{ch}) and slope (max. and min. ranges) are enforced during training.

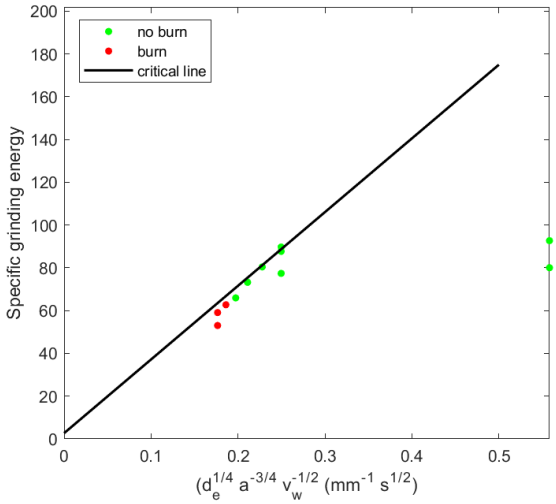

Fig. 7 The Critical Temperature Line (CTL) model classifies into “no burn” and “burn” points

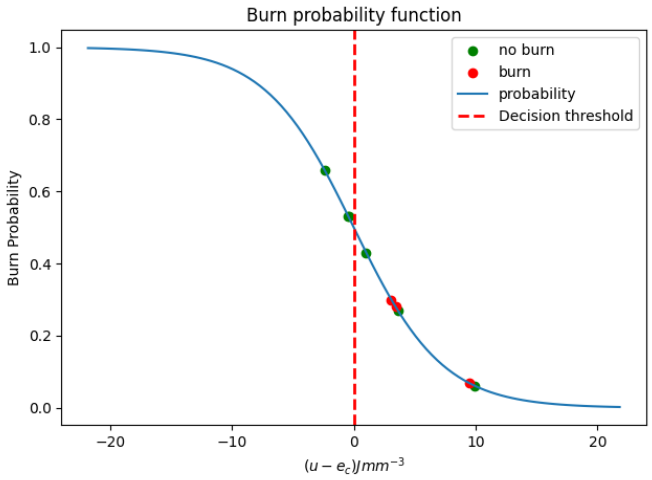

Fig. 8: Burn probability mapping from energy gap $(u - e_c)$ using the sigmoid function

Table 10 Process models developed to complete the grinding model

	Model	
Grinding ratio [6, 36]	$G = 14.0\, h_{eq}^{-0.13}$	(31)
Surface roughness [57]	$\mathrm{R_a} = \begin{cases} 0.4587 T_{ave}^{0.30} \; for \; 0 < T_{ave} < 0.254 \\ 0.7866 T_{ave}^{0.72} \; for \; 0.254 < T_{ave} < 2.54 \end{cases}$ where	(32)
	$T_{ave} = 11.095\, d_s^{\frac{4}{7}} a^{\frac{5}{7}} v_s^{\frac{1}{7}}$	(33)
Force [28]	$F_t = 5.749\, a^{0.896} v_w^{0.667} d_s^{-0.151}$	(34)
Specific energy [28]	$u = \frac{P}{Q}$	
Power [28]	$P = F_t v_s$	(36)
Burn detection [11]	$Burn = \begin{cases} False, & u < e_c \\ True, & u > e_c \end{cases}$ where	(37)
	$e_c = 2.70 + 43.75\, d_e^{1/4} a_e^{-3/4} v_w^{-1/2}$ and	(38)
	$P\{burn\} = \sigma(u - e_c) = \frac{1}{1 + e^{-(u - e_c)}}$	(39)

5.5 Optimization and parameter search

With the grinding model established, we proceed to parameter selection using both gradient descent and evolutionary algorithms. These optimization methods were chosen for their broad applicability and effectiveness across a wide range of problems, serving our purpose of illustrating the integration of burn cost and probability into the selection process. The specific process parameters and conditions for the case study are detailed in **Table 11**.

Table 11 Process specifications

Parameter	Unit	Constraint
Final surface roughness value, R_a	μm	≤ 1.8
Surface burn, B_i	True/False	False
No. of passes, N	-	[2, 10]
Total cut depth, a_{eT}	mm	2.00

The interior point algorithm [59] is selected as the gradient descent-based optimization method due to its widespread use and built-in availability in MATLAB® [60]. Specifically, MATLAB's *fmincon* function – designed for nonlinear constraint optimization – is employed and configured with the following settings: constraint tolerance and optimality tolerance are each set to 10^{-6}, step tolerance is set to 10^{-10}, maximum number of iterations set to 10^3, and maximum function evaluations set to 3000.

Since the total number of passes N is a discrete integer variable, it is not directly compatible with continuous gradient-based optimization. To address this, a line search is performed over the possible integer values of N. In the case study, N is explored over the range $2 \leq N \leq 10$. This is illustrated in the accompanying pseudocode.

Algorithm: Parameter selection using constraint nonlinear optimization

Input candidate solution X = $[v_{w,r}, a_r, v_{s.r}, n_r, v_{w,f}, a_f, v_{s,f}]$, cost function $J(X)$, and maximum no. of passes N

function BCM_SEARCH*(X, J, N)*
  $Y \leftarrow []$ Initialize set of solutions
  for $n_r \leftarrow 1$ to $N - 1$ **do**
    exclude n_r from solution
    $x \leftarrow [v_{w,r}, a_r, v_{s.r}, v_{w,f}, a_f, v_{s,f}]$
    $n \leftarrow no.of\ iterations$
    for $i \leftarrow 1$ to n **do**
      $\nabla \leftarrow \Delta x J(x)$
      $x \leftarrow x - \propto \nabla$
      if $|J(x) - J(x')| < \in$ **then**
        terminate loop
      end if
    end for
    Add solution x to set Y
    $Y += x \leftarrow [v_{w,r}, a_r, v_{s.r}, v_{w,f}, a_f, v_{s,f}]$
  end for
  $X \leftarrow best\ in\ set\ Y$
end function

Output X

For the evolutionary optimization approach, MATLAB®'s Genetic Algorithm (GA) function from the Optimization Toolbox [60] is used. The algorithm is configured with a constraint tolerance of 10^{-3}, a scattered crossover strategy, and a crossover fraction of 0.8. The population size is set to 70, with a migration fraction of 0.2. The mutation function is configured as Gaussian, and the maximum generations is set to 50.

Only these two optimization methods are explored due to their broad applicability across a wide range of problems. As demonstrated in the results, our intent was not to compare the performance of the optimization algorithms themselves, but rather to evaluate and contrast the underlying burn avoidance strategies.

6 Results and discussion

This section presents the results of applying two parameter selection strategies: the burn constraint approach and the burn cost probabilistic model. As previously established, thermal damage plays a critical role in grinding, and treating it as a simple constraint may not fully capture its impact. To evaluate the differences, both approaches are applied to the same experimental data and compared based on their performance outcomes. Using the models developed in earlier experiments, we examine and contrast the solutions yielded by each method.

6.1 Model evaluation summary

The model developed in this work is based on several simplifications and assumptions. In the process cost model, for example, the cost of wheel dressing is excluded—an acceptable simplification, as dressing frequency and cost are generally constant for a given workpiece. Wheel wear cost is modeled as inversely proportional to the grinding ratio, using the formulations in Equations (13) and (14).

The grinding ratio model itself is derived from just two data points, which, while sufficient to determine model coefficients, does not allow for a robust evaluation of model accuracy. For other components – such as force, power, and burn detection – 15 experimental data points were used, offering a higher degree of confidence. The force model achieved a coefficient of determination R^2 of 0.991, indicating strong predictive performance. The burn model, while not evaluated quantitatively, was visually assessed to produce a clear and effective separation between "burn" and "no burn" classifications.

Overall, these models represent approximations – our best effort to construct a grinding system model adequate for analyzing and comparing the two burn avoidance strategies, which is the central aim of this work. We acknowledge that with additional data, the accuracy and reliability of our results could be further improved.

6.2 Limitations of threshold-based thermal damage avoidance

Grinding operations inherently involve significant heat generation, and as previously discussed, the method used to account for thermal effects – particularly surface burn – can greatly influence cost-efficiency outcomes. To illustrate the limitations of the threshold-based approach in comparison to the burn cost approach, 3D plots of the resulting solutions from both methods are presented in Fig. 9. Each plot projects the search space onto a 2D plane defined by rough grinding work speed $v_{w,r}$ and cut depth a_r, highlighting the optimal solution within the feasible region. Both optimization approaches use the same burn detection model, as described in section 4, ensuring a consistent basis for comparison.

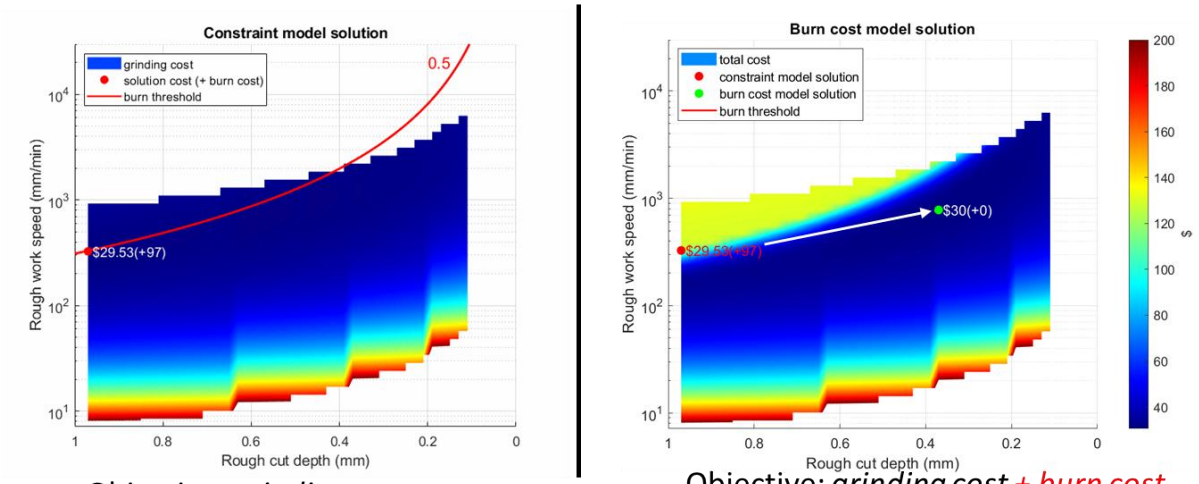

Fig. 9 Projected search space plots of **(L)** grinding cost vs rough cut depth showing the burn constraint threshold (red line) and solution (red dot), and **(R)** total cost depicting the burn cost model solution (green dot) as more robust to input sensitivity than the burn constraint solution (red dot).

Under the traditional constraint threshold approach (Fig. 9a), the optimal solution tends to lie near the threshold (red) line. This occurs due to the competing influences of minimizing cost and avoiding thermal damage. However, positioning the solution so close to the burn threshold indicates high sensitivity to input variations – small perturbations in system parameters could easily shift a "no burn" condition into a "burn" state. In such cases, the solution cannot be considered truly optimal, as the associated burn cost becomes significant. This highlights a key limitation of binary burn classification: it fails to capture the nuances of thermal risk.

Instead of treating burn as a binary outcome (burn or no burn), it is more appropriate to consider a spectrum of risk levels. The burn probability framework introduces this needed granularity, allowing for more informed and resilient decision-making in parameter selection. Fig. 9b illustrates this shift, showing the movement from the threshold-based optimal (red dot) to the burn cost-based optimal (green dot), which lies in a lower-risk region of the parameter space.

To address the limitation of integer variables in gradient descent, a line search is performed over a range of values for the number of passes, N. Fig. 10a visualizes this search, showing total cost as a function of N. As N decreases, the grinding cost initially drops, reaching an optimal point, beyond which further reductions in N lead to cost increases. This is due to the need for higher feed rates and deeper cuts, which accelerate wheel wear and increase energy consumption. This trade-off persists regardless of the risk threshold setting, as seen in Fig. 10b.

Fig. 10b presents the impact of varying burn risk thresholds – 0.1, 0.3, 0.5, and 0.7 – on the optimal number of passes. Across all thresholds, the optimal N consistently falls between three and six. Beyond this range, reducing N leads to sharp cost increases, particularly under lower risk tolerances. This supports the principle that tighter constraints on burn risk raise overall grinding costs, while higher risk tolerances allow more aggressive, and therefore cheaper, grinding strategies.

Collectively, these findings reveal that constraint-based burn avoidance acts merely as a filtering mechanism, excluding risky parameters but failing to account for cost-risk trade-offs. In contrast, the burn cost model provides a continuous measure of risk based on proximity to the burn threshold, enabling more nuanced and cost-effective decision-making. This approach aligns with practical burn risk

management and serves as the core motivation for adopting a burn cost framework in thermal damage avoidance.

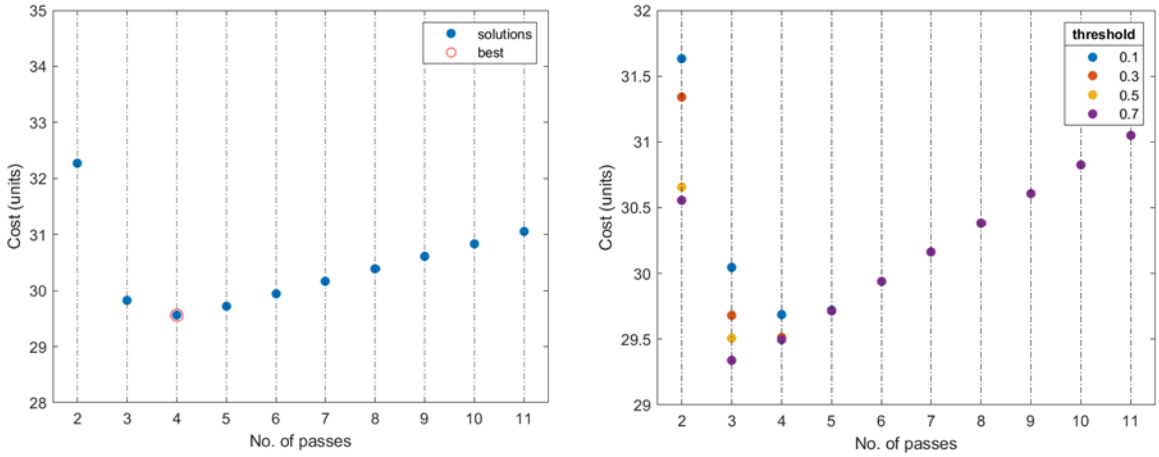

(a) (b)

Fig. 10 Line search plot showing grinding cost per specified number of passes N under **(a)** the traditional burn constraint strategy, with optimum at four, ($N = 4$). **(b)** varying burn thresholds. Trend is consistent but reflects influence of burn threshold on selection outcomes.

6.3 Cost profiles of the burn cost model and constraint model approaches

The two burn avoidance strategies are compared based on grinding cost alone (excluding burn cost) and total cost (which includes the cost of thermal damage). As shown in Fig. 11a, the burn constraint approach (red) exhibits a substantial difference between grinding cost and total cost—highlighting the hidden impact of thermal damage. In contrast, the burn cost model (green, Fig. 11b) results in a negligible difference—less than $3 per part—between grinding and total cost, indicating better alignment between optimization and actual outcomes.

The burn cost model exposes the often-overlooked financial impact of thermal damage, which is critical to achieving true cost efficiency. In the constraint-based approach, where burn cost is excluded, the total cost per part can be nearly three times higher than that of the burn cost model—approximately $90 versus $30 at four and six passes, respectively. This is despite both approaches yielding similar grinding costs.

These findings underscore the importance of explicitly incorporating burn cost into the optimization objective. While traditional approaches may appear cost-effective based on grinding parameters alone, they overlook the significant hidden costs associated with thermal damage. The burn cost model, by contrast, provides a more comprehensive and economically sound strategy for minimizing total cost.

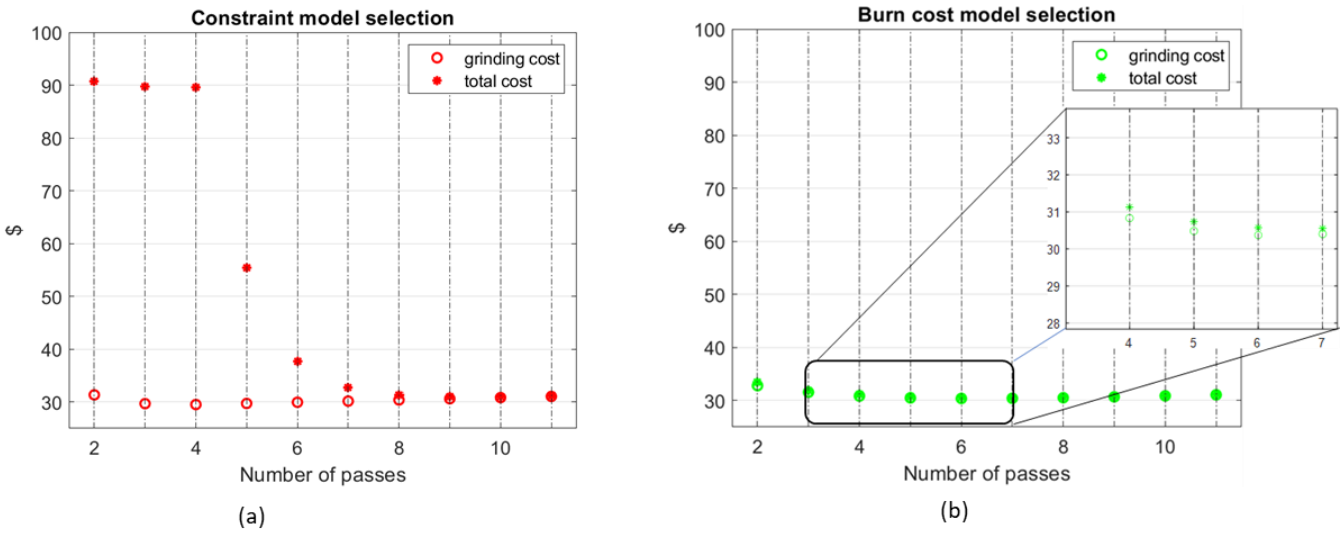

Fig. 11 Comparisons between the traditional burn constraint approach and the burn cost approach across the number of passes.

Further comparisons in Fig. 12 reveal patterns consistent with practical cost minimization strategies. In the rough grinding stage, both approaches yield similar parameter values, with the burn cost model (green) opting for slightly slower work speeds. However, significant differences appear in the finish stage, where the burn cost approach selects noticeably slower work speeds, indicating a preference for longer cycle times. This suggests a deliberate tradeoff: sacrificing speed to minimize the risk – and associated cost – of thermal damage. In contrast, the burn constraint approach (red) tolerates higher thermal risk to reduce machining time.

This outcome aligns with the well-established speed-quality tradeoff in manufacturing: while high material removal rates may lower immediate machining costs, they increase the likelihood of surface burn, ultimately compromising product quality and incurring higher total costs.

Interestingly, although we initially expected the burn cost model to favor lower cut depths, the results show that it actually selects higher cut depths than the constraint-based approach. However, when considering removal rate—the product of work speed and cut depth—it becomes clear that the burn cost model still favors a more conservative strategy. The lower removal rates observed under the burn cost model support the notion that removal rate is a key contributor to thermal damage risk and, by extension, to overall cost efficiency and product quality.

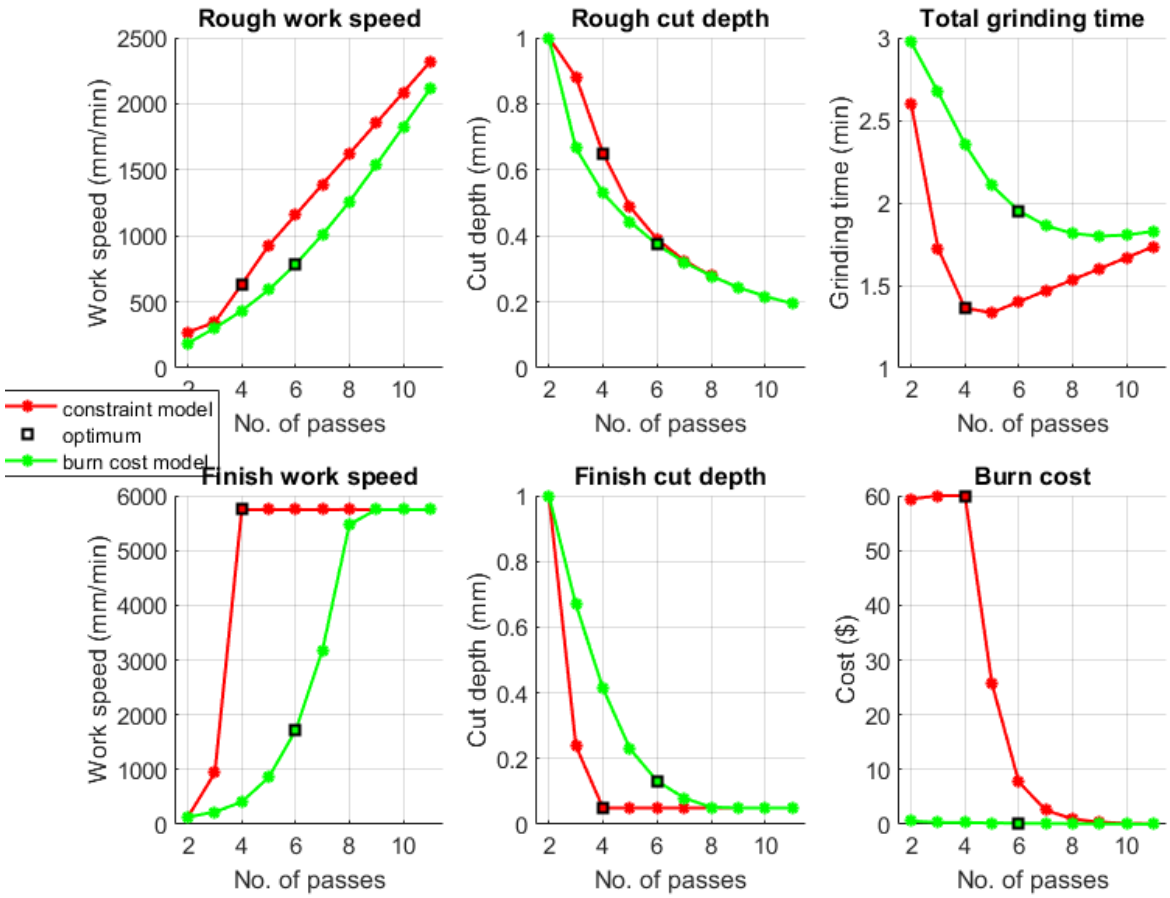

Fig. 12 Parameter values of selections for constraint model approach and burn cost model approach. *Work speeds and cut depths are higher in the rough stage for the constraint approach.*

Table 12 compares the optimal parameter selections of both strategies – represented by the square markers – at four passes for the burn constraint approach and six passes for the burn cost approach. The entire total cost difference between the two strategies, amounting to $60 per part, is attributable to burn cost.

In the burn cost approach, the solution consists of five rough passes and a significantly slower finish work speed (1,714 mm/min) compared to the burn constraint approach's three rough passes and much higher finish speed (5,745 mm/min). This slower finish speed in the burn cost approach increases the grinding time by about 45 seconds, but delivers a substantial reduction in burn risk, accounting for the $60 per part savings in total cost.

Such fine-tuned parameter selection – balancing grinding cost, burn cost, and cycle time – becomes possible only when burn cost is explicitly included in the optimization objective.

Table 12 Optimal parameter selections of traditional strategy and burn cost approach

			Standard	Burn-adjusted
Rough	work speed, mm/min	$v_{w,r}$	633	785
	cut depth, mm	a_r	0.650	0.374
	wheel speed, m/s	$v_{s,r}$	70	70
	No. of rough passes	n_r	3	5
Finish	work speed, mm/min	$v_{w,f}$	5745	1714
	wheel speed, m/s	$v_{s,f}$	70	70
Grinding time (min)			1:21	2:06
Grinding cost ($)			29.51	30.37
Burn cost ($)			60.00	0.20
Total Cost ($)			**89.51**	**30.57**

6.4 Sensitivity analysis of burn cost model approach

For the burn cost approach results, we evaluated the sensitivity of total cost to adjustments in work speed, cut depth, and number of passes N, with the number of rough passes defined as $n_r = N - 1$. The most pronounced sensitivity arose from reducing N (and consequently n_r), which increased the burn cost from $0.20 (baseline) to $5.60 per part. This result is expected, as fewer passes – and the corresponding higher removal rates – tend to elevate the risk of burn.

All other parameter changes remained within system constraints, with the only negligible effect ($0.02 per part) resulting from increasing the finish work speed by 300 mm/min. These results demonstrate that the burn cost approach is robust to typical operational variations, maintaining low burn costs even under moderate parameter shifts. Achieving a similar level of robustness with the burn constraint approach would require far greater complexity in its formulation and tuning.

Table 13 Sensitivity analyses on selections under the burn cost model approach

		Sensitivities (+/-)	Total cost ($)	Burn cost ($)	Time (mm:ss)	Parts/hr
Reference (burn cost model solution)			30.57	0.20	01:57	30.8
Rough	work speed, mm/min	$\mathbf{v_{w,r} - 300}$	31.95	0.00	02:49	21.2
		$\mathbf{v_{w,r} + 300}$	32.85	2.83	01:33	38.5
	cut depth, mm	$\mathbf{a_r - 0.05}$	30.57	0.20	01:57	30.8
		$\mathbf{a_r + 0.05}$	30.57	0.20	01:57	30.8
	No. of rough passes	$\mathbf{n_r - 1}$	35.46	5.60	01:36	37.5
		$\mathbf{n_r + 1}$	31.03	0.01	02:18	26.1
Finish	work speed, mm/min	$\mathbf{v_{w,f} - 300}$	30.63	0.20	01:58	30.3
		$\mathbf{v_{w,f} + 300}$	30.54*	0.20	01:55	31.1
	cut depth, mm	$\mathbf{a_f - 0.05}$	30.72	0.31	01:57	30.8
		$\mathbf{a_f + 0.05}$	30.49	0.13	01:57	30.8

* slight violation of the surface roughness constraint R_a

6.5 Burn cost model under varying workpiece value

The monetary cost of burn – defined as the product of burn probability and workpiece value – provides a direct way to integrate value considerations into the parameter selection process. Under the traditional burn constraint approach, such considerations are either absent or indirectly enforced through fixed risk thresholds, which rarely align with the actual workpiece value.

Fig. 13 illustrates the cost implications for workpiece values ranging from $0 to $200. As workpiece value increases, both grinding cost and total cost rise due to a significant reduction in burn risk (yellow line). In practice, expensive parts naturally prompt more cautious grinding – slower removal rates, shallower cuts, and more passes – even though the basic act of grinding costs the same for cheap and expensive workpieces. The burn cost approach reproduces this expected behavior by intentionally slowing the process to mitigate risk for high-value parts. This aligns with real-world practice – costly workpieces demand greater care under the same threat of thermal damage.

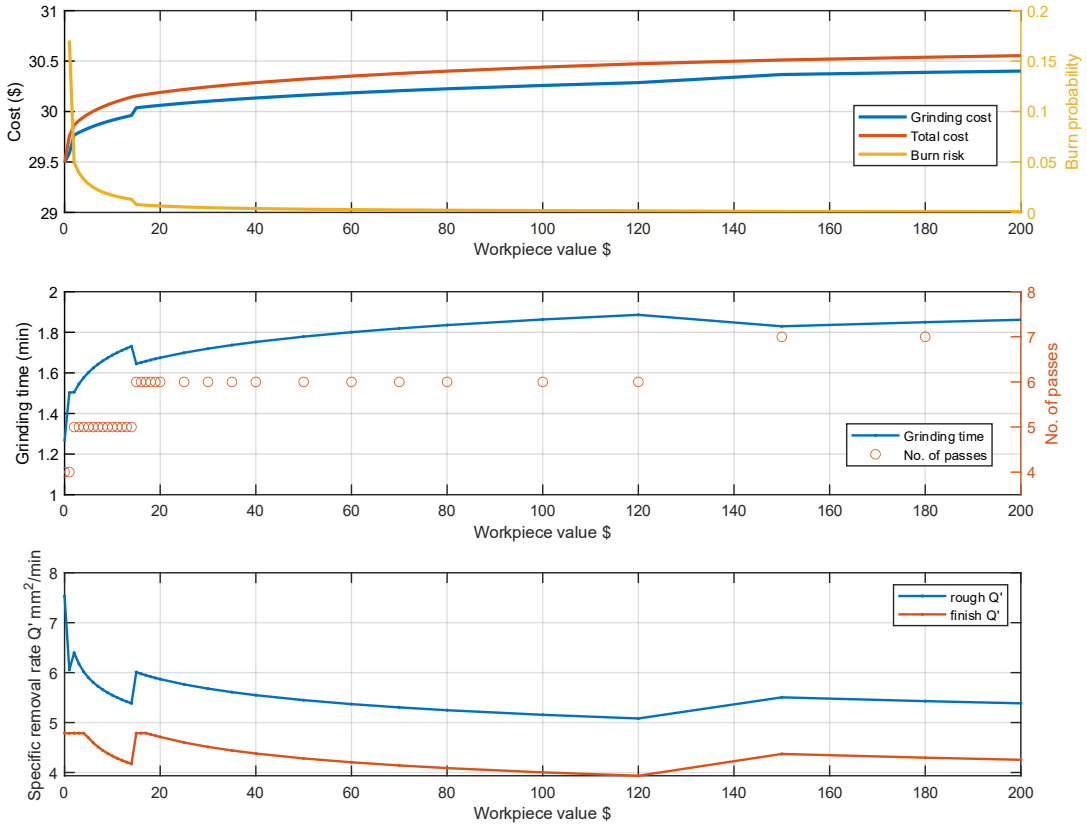

Fig. 13 Optimal grinding and total costs under varying workpiece value. As workpiece value increases, the algorithm prioritizes reducing burn risk over minimizing grinding cost. This trade-off is achieved through lower removal rates, longer grinding times, and a greater number of passes.

The total cost increase reflects these added precautions: more passes, lower removal rates, and reduced tolerance for burn risk. This trade-off manifests as longer grinding times (slower work speeds) and shorter cuts per pass. At the same time, speeds are not reduced excessively, as prolonged wheel-workpiece contact can increase heat transfer and raise burn risk.

When comparing the traditional threshold-based burn avoidance with the burn cost model, several key insights emerge. First, the threshold approach fails to reflect real-world decision-making as accurately as the burn cost method. The burn cost approach incorporates thermal damage risk directly into the optimization objective through a comprehensive total cost analysis. Second, the use of burn probability enables explicit estimation of burn costs, allowing their seamless integration into the cost minimization process. Third, by accounting for burn risk in its decision-making, the burn cost approach produces solutions that are inherently more robust than those derived from a fixed threshold line. Finally, the burn cost model is adaptive to workpiece value, an essential factor in achieving true grinding cost efficiency.

The grinding burn cost model presented in this study demonstrates clear potential for improving overall machining cost efficiency. By replacing traditional threshold-based methods with a probability-weighted cost approach, we identified parameter selections that minimize total process cost more effectively. These findings, however, are based on models that incorporate certain simplifications and assumptions. While the grinding system model was designed to represent a wide range of configurations, and the burn model was assumed to estimate burn occurrence and burn probability with equal accuracy, these assumptions impose limitations. Even so, the burn cost approach provides a promising and broadly applicable framework for mitigating thermal damage. Incorporating more extensive datasets and refining the underlying models in future work would further improve the reliability and generalizability of the results.

Conclusion

Surface grinding optimization must account for thermal damage risk and its substantial cost implications. Compared to the traditional constraint-based approach, our burn cost estimation framework more effectively aligns with the true optimization objective. By incorporating the concept of burn probability into our analysis, we provided a practical means of quantifying thermal risk and translating it into cost, enabling more accurate evaluation of total grinding costs. Our results demonstrate that incorporating burn cost adjustments minimizes both production expenses and thermal damage losses, supporting the overarching goal of cost efficiency.

The investigation into thermal damage dynamics and their influence on parameter selection produced findings consistent with practical observations. First, while thermal thresholds can be effective, they involve notable cost trade-offs that burn cost estimation can balance more effectively. Second, although the burn cost model often recommends slower removal rates than the constraint approach, its selections are better tuned to mitigate burn risk. Third, by explicitly quantifying risk through burn probability, the burn cost model yields parameter choices that are more robust to process uncertainties.

A promising application of this approach lies in real-time process control, where adapting grinding parameters to changing burn risk could yield significant benefits. Here, probability-based burn cost modeling can provide actionable guidance, although sensor resolution and computation rates may impose practical constraints.

Future work could extend robustness analysis to multi-stage strategies involving roughing, pre-finishing, and finishing passes. Additional process variables – such as coolant flow rate, abrasive wheel composition, and integrated thermal profiling – may further enhance optimization. With larger and more diverse datasets, burn models could achieve greater accuracy in predicting burn probability and estimating risk. This study provides a solid foundation for advancing comprehensive, risk-aware strategies in surface grinding optimization.

Declarations

The authors declared no potential conflicts of interest with respect to the research, authorship, and/or publication of this article. This work was supported by Precision Surface Solutions. The authors declare that no funds, grants, or other support were received during the preparation of this manuscript.

References

1. Field M, Kegg R, Buescher S (1980) Computerized cost analysis of grinding operations. CIRP Annals 29:233–237. https://doi.org/10.1016/S0007-8506(07)61328-6
2. Wen XM, Tay AAO, Nee AYC (1992) Micro-computer-based optimization of the surface grinding process. J Mater Process Technol 29:75–90. https://doi.org/10.1016/0924-0136(92)90426-S
3. Hadi M, Mahmood G, Azizi R, Gholami MH, Azizi MR (2014) Constrained grinding optimization for time, cost, and surface roughness using NSGA-II. The International Journal of Advanced Manufacturing Technology 73:981–988. https://doi.org/10.1007/S00170-014-5884-6
4. Maier M, Rupenyan A, Bobst C, Wegener K (2020) Self-optimizing grinding machines using Gaussian process models and constrained Bayesian optimization. International Journal of Advanced Manufacturing Technology 108:539–552. https://doi.org/10.1007/S00170-020-05369-9
5. Lee CW, Shin YC (2000) Evolutionary modelling and optimization of grinding processes. Int J Prod Res 38:2787–2813. https://doi.org/10.1080/002075400411484
6. Choi T, Shin YC (2007) Generalized intelligent grinding advisory system. Int J Prod Res 45:1899–1932. https://doi.org/10.1080/00207540600562025
7. Brinksmeier E, Aurich JC, Govekar E, Heinzel C, Hoffmeister HW, Klocke F, Peters J, Rentsch R, Stephenson DJ, Uhlmann E, Weinert K, Wittmann M (2006) Advances in modeling and simulation of grinding processes. CIRP Annals 55:667–696. https://doi.org/10.1016/J.CIRP.2006.10.003
8. Kruszynski BW, van Luttervelt CA (1991) An attempt to predict residual stresses in grinding of metals with the aid of a new grinding parameter. CIRP Annals 40:335–337. https://doi.org/10.1016/S0007-8506(07)62000-9
9. Hamdi H, Zahouani H, Bergheau JM (2004) Residual stresses computation in a grinding process. J Mater Process Technol 147:277–285. https://doi.org/10.1016/S0924-0136(03)00578-8
10. Lazoglu I, Ulutan D, Alaca BE, Engin S, Kaftanoglu B (2008) An enhanced analytical model for residual stress prediction in machining. CIRP Annals 57:81–84. https://doi.org/10.1016/J.CIRP.2008.03.060
11. Malkin S, Guo C (2007) Thermal analysis of grinding. CIRP Ann Manuf Technol 56:760–782. https://doi.org/10.1016/j.cirp.2007.10.005
12. Rowe WB, Jin T (2001) Temperatures in high efficiency deep grinding (HEDG). CIRP Annals 50:205–208. https://doi.org/10.1016/S0007-8506(07)62105-2
13. Khazi I, Kovacs A, Mescheder U, Zahedi A, Azarhoushang B (2021) Fusion of optical and microfabricated eddy-current sensors for the non-destructive detection of grinding burn.

Advances in Science, Technology and Engineering Systems Journal 6:1414–1421. https://doi.org/10.25046/AJ0601160
14. Kovacs A, Khazi I, Zahedi A, Mescheder U, Azarhoushang B (2020) Development of an optical sensor for the non-destructive testing of grinding burn. Proceedings of IEEE Sensors 2020-Octob: https://doi.org/10.1109/SENSORS47125.2020.9278837
15. Sauter E, Sarikaya E, Winter M, Wegener K (2021) In-process detection of grinding burn using machine learning. International Journal of Advanced Manufacturing Technology 115:2281–2297. https://doi.org/10.1007/S00170-021-06896-9/FIGURES/14
16. Yang Z, Wu H, Yu Z, Huang Y (2014) A non-destructive surface burn detection method for ferrous metals based on acoustic emission and ensemble empirical mode decomposition: from laser simulation to grinding process. Meas Sci Technol 25:035602. https://doi.org/10.1088/0957-0233/25/3/035602
17. Benardos PG, Vosniakos GC (2003) Predicting surface roughness in machining: A review. Int J Mach Tools Manuf 43:833–844. https://doi.org/10.1016/S0890-6955(03)00059-2
18. Amitay G, Malkin S, Koren Y (1981) Adaptive control optimization of grinding. Journal of Engineering for Industry 103:103–108. https://doi.org/10.1115/1.3184449
19. Lee CW (2009) Dynamic optimization of the grinding process in batch production. J Manuf Sci Eng 131:0210061–0210096. https://doi.org/10.1115/1.3090880/468435
20. Lee CW (2008) Estimation strategy for a series of grinding cycles in batch production. IEEE Transactions on Control Systems Technology 16:556–561. https://doi.org/10.1109/TCST.2007.908225
21. Nametala CAL, Souza AM, Pereira Júnior BR, da Silva EJ (2020) A simulator based on artificial neural networks and NSGA-II for prediction and optimization of the grinding process of superalloys with high performance grinding wheels. CIRP J Manuf Sci Technol 30:157–173. https://doi.org/10.1016/J.CIRPJ.2020.05.004
22. Warren Liao T, Chen LJ (1994) A neural network approach for grinding processes: Modelling and optimization. Int J Mach Tools Manuf 34:919–937. https://doi.org/10.1016/0890-6955(94)90025-6
23. Lee CW, Choi T, Shin YC (2003) Intelligent model-based optimization of the surface grinding process for heat-treated 4140 steel alloys with aluminum oxide grinding wheels. J Manuf Sci Eng 125:65–76. https://doi.org/10.1115/1.1537738
24. Kishore K, Chauhan SR, Kumar Sinha M (2024) A comprehensive investigation on eco-benign grindability improvement of Inconel 625 using nano-MQL. Precis Eng 90:81–95. https://doi.org/10.1016/J.PRECISIONENG.2024.08.004
25. Rowe WB (2001) Thermal analysis of high efficiency deep grinding (HEDG). Int J Mach Tools Manuf 41:1–19. https://doi.org/10.1016/S0890-6955(00)00074-2
26. Bell A, Jin T, Stephenson DJ (2011) Burn threshold prediction for High Efficiency Deep Grinding. Int J Mach Tools Manuf 51:433–438. https://doi.org/10.1016/J.IJMACHTOOLS.2011.01.006
27. Batako ADL, Morgan MN, Rowe BW (2012) High efficiency deep grinding with very high removal rates. The International Journal of Advanced Manufacturing Technology 66:1367–1377. https://doi.org/10.1007/S00170-012-4414-7
28. Rowe BW (2013) Principles of modern grinding technology, 2e ed. Elsevier Inc

29. Carslaw HS, Jaeger JC (1962) Conduction of heat in solids. Phys Today 15:74–76. https://doi.org/10.1063/1.3057871
30. Heinzel C, Heinzel J, Guba N, Hüsemann T (2021) Comprehensive analysis of the thermal impact and its depth effect in grinding. CIRP Annals 70:289–292. https://doi.org/10.1016/J.CIRP.2021.04.010
31. Kishore K, Sinha MK, Singh A, Archana, Gupta MK, Korkmaz ME (2022) A comprehensive review on the grinding process: Advancements, applications and challenges. Journal of Mechanical Engineering Science 236:10923–10952. https://doi.org/10.1177/09544062221110782
32. Lanzagorta JL, Urgoiti L, Vazquez PR, Barrenetxea D, Sánchez JA (2020) Experimental approach for a grinding burn in-process inspection system based on Eddy Current. Procedia CIRP 87:391–396. https://doi.org/10.1016/J.PROCIR.2020.02.011
33. He B, Wei C, Ding S, Shi Z (2019) A survey of methods for detecting metallic grinding burn. Measurement 134:426–439. https://doi.org/10.1016/J.MEASUREMENT.2018.10.093
34. Guo W, Li B, Shen S, Zhou Q (2019) An intelligent grinding burn detection system based on two-stage feature selection and stacked sparse autoencoder. International Journal of Advanced Manufacturing Technology 103:2837–2847. https://doi.org/10.1007/S00170-019-03748-5
35. Khosravi M, König C, Maier M, Smith RS, Lygeros J, Rupenyan A (2023) Safety-aware cascade controller tuning using constrained Bayesian optimization. IEEE Transactions on Industrial Electronics 70:2128–2138. https://doi.org/10.1109/TIE.2022.3158007
36. Snoeys R, Peters J, Decneut A (1974) Significance of chip thickness in grinding. CIRP Annals 23:227–237
37. Kota SS, Balguri PK, Govardhan D (2022) Optimization of grinding depth to avoid grind-induced burns in 35NCD16 alloy. Mater Today Proc 62:2739–2743. https://doi.org/10.1016/J.MATPR.2021.12.122
38. Jamshidi H, Budak E (2022) A digital twin-based framework for selection of grinding conditions towards improved productivity and part quality. Journal of Intelligent Manufacturing 2022 1–13. https://doi.org/10.1007/S10845-022-02031-X
39. Sauter E, Winter M, Wegener K (2022) Analysis of robustness and transferability in feature-based grinding burn detection. The International Journal of Advanced Manufacturing Technology 2022 120:2587–2602. https://doi.org/10.1007/S00170-022-08834-9
40. Afsari A, Ramezani M, Heidari S, Karimisharifabadi J (2020) Imperialist competitive algorithm (ICA) approach for optimization of the surface grinding process. Journal of Modern Processes in Manufacturing and Production 9:51–62. https://doi.org/20.1001.1.27170314.2020.9.1.5.7
41. Debnath S, Doloi B, Bhattacharyya - B, Kumar Arya R, Paliwal S, Dvivedi A, Akintseva A V, Prokhorov A V, Omelchenko S V (2020) Methodology for designing optimal internal grinding cycles resistant to varying processing conditions. IOP Conf Ser Mater Sci Eng 709:033004. https://doi.org/10.1088/1757-899X/709/3/033004

42. Pereverzev PP, Akintseva A V., Alsigar MK (2019) Use of dynamic programming method to design for optimal performance of grinding cycles. Lecture Notes in Mechanical Engineering 0:1709–1714. https://doi.org/10.1007/978-3-319-95630-5_183
43. Kumar Patel D, Goyal D, Pabla BS (2018) Optimization of parameters in cylindrical and surface grinding for improved surface finish. R Soc Open Sci 5:. https://doi.org/10.1098/RSOS.171906
44. Steffan M, Haas F, Pierer A, Jens G (2017) Adaptive grinding process-prevention of thermal damage using OPC-UA technique and in situ metrology. Journal of Manufacturing Science and Engineering, Transactions of the ASME 139:. https://doi.org/10.1115/1.4038123
45. Jiang J, Ge P, Sun S, Wang D, Wang Y, Yang Y (2016) From the microscopic interaction mechanism to the grinding temperature field: An integrated modelling on the grinding process. Int J Mach Tools Manuf 110:27–42. https://doi.org/10.1016/j.ijmachtools.2016.08.004
46. Wegener K, Baumgart C (2018) Grinding burn. CIRP Encyclopedia of Production Engineering 1–7. https://doi.org/10.1007/978-3-642-35950-7_16786-1
47. Lavisse B, Weiss L, Kokanyan N, Lefebvre A, Henrion E, Sinot O, Tidu A (2022) Investigations of grinding burn on a nitrided steel. Procedia CIRP 108:549–554. https://doi.org/10.1016/J.PROCIR.2022.03.086
48. Malkin S (1989) Grinding technology: theory and applications of machining with abrasives. Ellis Horwood, Chichester, UK
49. Sinha MK, Kishore K, Sharma P (2025) Surface integrity evaluation in ecological nanofluids assisted grinding of Inconel 718 superalloy. Proceedings of the Institution of Mechanical Engineers, Part E: Journal of Process Mechanical Engineering 239:75–86. https://doi.org/10.1177/09544089231171042/FORMAT/EPUB
50. Lindsay RP (1973) On the surface finish-metal removal relationship in precision grinding. Journal of Engineering for Industry 95:815–820. https://doi.org/10.1115/1.3438231
51. Kishore K, Chauhan SR, Sinha MK (2025) Investigation on Grindability Improvement of Inconel 625 using Multi-walled Carbon Nanotubes Nanofluids-Assisted Minimum Quantity Lubrication Surface Grinding. J Mater Eng Perform 34:6240–6251. https://doi.org/10.1007/S11665-024-09648-4/METRICS
52. Platt J (1999) Probabilistic outputs for support vector machines and comparisons to regularized likelihood methods. Advances in large margin classifiers 10:61–74
53. Li HX, Yang JL, Zhang G, Fan B (2013) Probabilistic support vector machines for classification of noise affected data. Inf Sci (N Y) 221:60–71. https://doi.org/10.1016/J.INS.2012.09.041
54. Pereverzev PP, Pimenov DY (2015) Optimization of control programs for numerically controlled machine tools by dynamic programming. Russian Engineering Research 35:135–142. https://doi.org/10.3103/S1068798X15020197
55. Li GF, Wang LS, Yang LB (2002) Multi-parameter optimization and control of the cylindrical grinding process. J Mater Process Technol 129:232–236. https://doi.org/10.1016/S0924-0136(02)00607-6
56. National Instruments Inc Data acquisition (DAQ) systems, devices & software - NI. https://www.ni.com/en/shop/data-acquisition.html. Accessed 28 Apr 2024

57. King RI, Hahn RS (1986) Handbook of Modern Grinding Technology, 1st ed. Springer New York, NY
58. Cortes C, Vapnik V (1995) Support-vector networks. Mach Learn 20:273–297. https://doi.org/10.1007/BF00994018
59. Zorkaltsev VI, Mokryi I V. (2018) Interior point algorithms in linear optimization. Journal of Applied and Industrial Mathematics 12:191–199. https://doi.org/10.1134/S1990478918010179
60. The Mathworks Inc. (2022) Optimization toolbox version: 9.4 (R2022b). https://www.mathworks.com/products/optimization.html. Accessed 31 Dec 2023